Kinetic pathways from embedded-atom-method potentials: Influence of the activation barriers

Yann Le Bouar* and Frédéric Soisson
Service de Recherches en Métallurgie Physique, DEN-DMN, CEA Saclay, 91191 Gif-sur-Yvette, France
(Received 25 July 2001; published 31 January 2002)

The precipitation kinetics in alloys is now widely studied at a microscopic scale, using Monte Carlo simulations and simple energetic and diffusion models. In the present paper, we first test the assumptions of these models, in the case of the copper precipitation in α-iron, using static relaxation of a many-body embedded-atom-method (EAM) potential. In dilute alloys, the EAM configurational energies can be described by simple pair interactions on rigid lattice. The EAM vacancy migration barriers are reproduced by saddle-point binding energies which are very sensitive to both the nature of the jumping atom and that of the first neighbors of the saddle point. Finally, these microscopic parameters are integrated in a Monte Carlo scheme. The dependence of the saddle-point binding energies on the local atomic configurations modifies the relative mobility of small Cu clusters and Cu monomers. At high temperature, it leads to a slowing down of the precipitation by a constant ratio of on the time scale, but at low temperature, the kinetic pathway is dramatically modified.

DOI: 10.1103/PhysRevB.65.094103 PACS number(s): 64.75.+g, 81.30.Mh

I. INTRODUCTION

The precipitation kinetics in alloys is now widely studied using Monte Carlo simulations. The first simulations were based on a very simple diffusion mechanism: the direct exchange of two nearest-neighbor atos [Kawazaki dynamics; see, e.g. (Ref. 1)]. Then more realistic diffusion mechanisms by vacancy jumps were introduced in the Monte Carlo method.[2,3] Recently, special attention has been paid to the influence of such diffusion mechanisms on the kinetic pathway during spinodal decomposition,[3–5] nucleation and growth,[5–7] or phase ordering.[8,9] Besides the different diffusion mechanisms, these studies have relied on different models to compute the activation barriers and attempt frequencies of the diffusion events and on different Monte Carlo algorithms (especially to get a physical estimation of the time).[10] However, in all these studies, the configurational energies and the activation barriers are computed using very simple potentials consisting of short-range pair interactions on a rigid lattice. More accurate (many-body and position-dependent) potentials exist, but properly taking into account the atomic relaxations dramatically decreases the computer efficiency.

In brief, most Monte Carlo studies of precipitation in alloys are based on severe assumptions, both when computing the configurational energies and the diffusion properties. These assumptions, and their consequences on the kinetics of phase transformations, have to be questioned and their validity should be tested by comparison with more accurate potentials.

In the present paper, we focus on the Fe-Cu system. Although pure Cu has a face-centered-cubic (fcc) structure, the first step of the Cu precipitation on the body-centered-cubic (bcc) lattice of α-Fe (when the precipitates radius is smaller than 2 nm) is fully coherent[11] and the lattice parameter of the metastable bcc Cu is almost the same as the one of Fe.[12–14] Monte Carlo simulations on rigid lattices have then been applied to this system.[15] Moreover, several Fe-Cu position-dependent potentials have been developed,[16–18] mainly to study the latter bcc to fcc transitions of Cu precipitates (e.g., Refs. 19 and 20).

In the first part of the paper, we use the embedded-atom-method (EAM) potential of Ludwig *et al.*[16] as a reference and investigate whether a simple rigid lattice model (RLM) can be built to reproduce both the configurational and kinetic properties predicted by this many-body potential. Then, the interaction energies and the saddle-point (SP) energies obtained with the EAM potential are integrated both in the theory of diffusion in dilute alloys and in a Monte Carlo scheme to study the diffusion properties of Cu impurities and small Cu clusters. The influence of the specific form of the saddle-point energy on the microstructural development is finally discussed in a third part.

II. RIGID LATTICE MODEL VERSUS EMBEDDED ATOM METHOD: CONFIGURATIONAL AND KINETIC PARAMETERS

In the present section, we assess whether the configurational energies of dilute $Fe_{1-x}Cu_x$ alloys predicted by the EAM potential can be accurately described by a rigid lattice model with pair interactions between first-nearest-neighbor atoms. Then, we show how the migration barriers of the rigid lattice model have to be chosen to reproduce the jump frequencies of the EAM potential.

A. Configuration energies in dilute $Fe_{1-x}Cu_x$ alloys

1. Prediction of the EAM potential

The first step of our study was to compute the relaxed energies of several configurations containing up to two Cu atoms and one vacancy as point defects in the α-Fe matrix. To do so, we have used the EAM potential of Ludwig *et al.*,[16] discretized over 3000 points between 0 and 5 Å. The intermediate values of the potential were obtained using a cubic spline interpolation. We have used a cubic α-Fe matrix containing 2000 or 5488 atoms with periodic boundary conditions, and the configurations were relaxed using a conjugate gradient algorithm allowing simultaneously the move-

TABLE I. Cohesive energies E^{coh}, the vacancy formation energy (E_V^{for}), the Cu solution energy E_{Cu}^{sol}, and binding energies (E^b) between first and second nearest neighbors in α-iron that we have obtained using the EAM potential of Ref. 16, compared with the results obtained by Osetsky *et al.* (Ref. 18) and by Ackland *et al.* (Ref. 17). The energies are given in eV per atom (* unrelaxed value).

	$E_{Fe}^{coh}(bcc)$	$E_{Cu}^{coh}(fcc)$	E_V^{for}	E_{Cu}^{sol}	$E_{Cu\text{-}V}^b(1)$	$E_{Cu\text{-}V}^b(2)$	$E_{Cu\text{-}Cu}^b(1)$	$E_{Cu\text{-}Cu}^b(2)$
EAM Ludwig *et al.*	4.28	3.54	1.63	0.50	-0.19	0.04	-0.20	0.02
Pseudo. Osetsky *et al.*	-	-	2.05	-	-0.14	-0.02	-0.20	-0.08
EAM Ackland *et al.*	4.316	3.519	1.70	0.317*	-0.087	-0.04	-0.075	-0.035

ment of atoms and an isotropic dilatation of the box. The relaxation was stopped when the sum of the square of the forces (in eV/Å) remaining on each atom was lower than 10^{-7} and, simultaneously, the error in the lattice parameter was lower than 10^{-8} Å. We have checked that the accuracy of this procedure on the configurational energies is better than 10^{-4} eV.

We first compute the energies of the six most simple configurations in dilute Fe-Cu alloys using the EAM potential,[16] i.e., the vacancy formation energy E_V^{for} and the Cu solution energy E_{Cu}^{sol} (Ref. 37) in α-Fe, the binding energies $E_{Cu\text{-}V}^b(1)$ and $E_{Cu\text{-}V}^b(2)$ between a Cu impurity and a vacancy in a first- and second-nearest-neighbor position, and the binding energies $E_{Cu\text{-}Cu}^b(1)$ and $E_{Cu\text{-}Cu}^b(2)$ between two Cu impurities in a first- and second-nearest-neighbor position. The results are summarized in Table I and compared with the results obtained by Ackland *et al.*[17] with another EAM potential and Osetsky *et al.*[18] with a pseudopotential approach.

Most interestingly, the binding energy for vacancy-Cu and Cu-Cu complexes decreases rapidly with the distance between the two point defects (i.e., Cu or V) and is negligible beyond a distance larger than the second coordination sphere. Moreover, to a good approximation (0.04 eV), our calculations show the Cu atom and vacancy only interact when they are in a first-nearest-neighbor position in the bcc crystal. As shown in Table I, this conclusion is in agreement with the results obtained by Osetsky *et al.*[18] and Ackland *et al.*[17] Finally, with our EAM potential the binding energy between second-nearest-neighbor Cu impurities $E_{Cu\text{-}Cu}^b(2)$ is negligible compared with that between first nearest neighbors. With the potentials developed by Osetsky *et al.*[18] and by Ackland *et al.*[17] the difference between $E_{Cu\text{-}Cu}^b(2)$ and $E_{Cu\text{-}Cu}^b(1)$ is less pronounced.

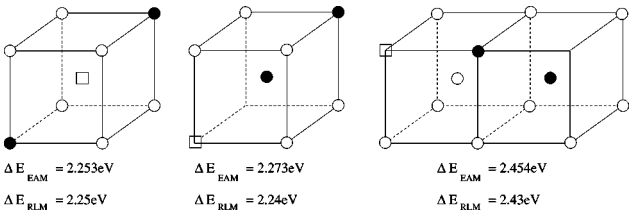

FIG. 1. Formation energies of three Cu-Cu-*V* complexes obtained with the rigid lattice model (RLM) and the relaxed EAM potential. The white and black circles are Fe and Cu atoms, respectively, and the position of the vacancy is shown by a white square.

2. Rigid lattice model approach

The above results suggest that the configurational energy of dilute Fe-Cu alloys may be computed using first-nearest-neighbor interactions only. To assess this point, we have compared the relaxed energies obtained with our EAM potential with a rigid lattice model with pair interactions between the first-nearest-neighbor atoms: $\epsilon_{FeFe}, \epsilon_{FeCu}$, and ϵ_{CuCu}. In such a model, the cohesive energy of pure iron is then given by

$$E_{Fe}^{coh} = -\frac{Z}{2}\epsilon_{FeFe}, \tag{2.1}$$

where $Z=8$ is the coordination number of the bcc lattice (the same equation stands for pure bcc copper).

If the model is limited to the three first-nearest-neighbors interactions $\epsilon_{FeFe}, \epsilon_{FeCu}$, and ϵ_{CuCu}, the vacancy formation energy in a pure metal E_V^{for} (experimental value 1.68 eV in α-iron[21]) is necessarily equal to the cohesive energy E^{coh} (experimental value 4.28 eV in α-iron). However, this drawback can be avoided, even within a first-nearest-neighbor-scheme, by introducing new interaction energies ϵ_{FeV} and ϵ_{CuV} between the vacancy and the surrounding atoms. Then

$$E_V^{\text{for}}(Fe) = -\frac{Z}{2}\epsilon_{FeFe} + Z\epsilon_{FeV}. \tag{2.2}$$

These vacancy-atom interactions (sometimes called "ghost" interactions) are a simple way to partly take into account the electronic relaxation around the vacancy.

Therefore, our rigid lattice model contains the five interactions energies ϵ_{FeFe}, ϵ_{FeCu}, ϵ_{CuCu}, ϵ_{FeV}, and ϵ_{CuV}, which have been chosen to reproduce the α-Fe cohesive energy and the formation, solution, and binding energies detailed in Table I. The obtained interaction energies are presented in Table II, together with the ones used by Soisson *et al.*[15] in their previous Monte Carlo study of the copper precipitation in iron. The two sets of parameters, obtained

TABLE II. Interaction energies (in eV) between first nearest neighbors in the bcc lattice given by our fit compared with the values used by Soisson *et al.* (Ref. 15).

	ϵ_{FeFe}	ϵ_{FeCu}	ϵ_{CuCu}	ϵ_{FeV}	ϵ_{CuV}
Present work	-1.070	-0.915	-0.960	-0.331	-0.366
Soisson *et al.*	-1.070	-0.980	-1.070	-0.330	-0.280

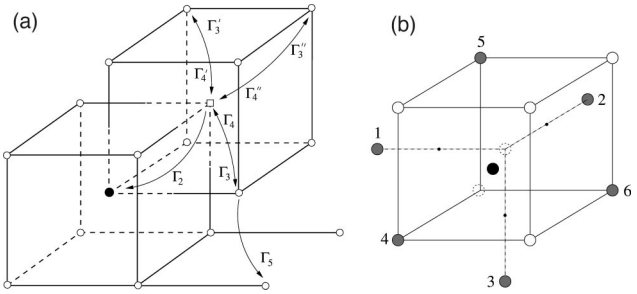

FIG. 2. (a) Definition of the jump frequencies Γ_i of a vacancy (white square) around a Cu impurity (black circle) used in the Le Claire model (Ref. 27). (b) Position of the six first-nearest-neighbor atoms (gray circles) of the saddle-point position (black circle). The dashed circles designate the initial and final positions of the atom during the jump.

with a similar fitting procedure, are rather close to each other (see the Appendix for a detailed comparison).

3. Test of the rigid lattice model

To test the validity of this RLM for dilute Fe-Cu alloys, we have computed the interaction of Cu dimers with a vacancy. Several of these configurations are drawn in Fig. 1. For the 12 configurations that we have studied, the difference in energy between the two models is always lower than 0.04 eV. This shows that the relaxation around the vacancy is reasonably well described by the ''ghost'' interactions between the vacancy and the atoms and that the introduction of second-nearest-neighbor interactions is not necessary.

As a second test of the RLM, we have computed the copper solubility limit C_s in α-Fe. We have estimated the energy of the solid solution using the regular solution model, and the entropy using the mean-field approach. It gives $C_s \sim \exp(Z\omega/2kT)$ at low temperature [i.e., for $T \ll T_c = -(Z\omega)/(4k)$], where $\omega = \epsilon_{FeFe} + \epsilon_{CuCu} - 2\epsilon_{FeCu}$ is the mixing energy and $Z=8$ the coordination number. At 500 K, the solubility limit predicted by this rigid lattice model is $C_s \approx 10^{-8}$. Thus, the model correctly reproduces a very low solubility of copper in iron.[22]

As a conclusion, the configurational energy of dilute Fe-Cu alloys can reasonably be described by a rigid lattice model with pair interactions between first nearest neighbors, provided that ghost interactions are introduced between the vacancy and the atoms.

B. Migration barriers and saddle point energies in dilute Fe-Cu alloys

The present section deals with the diffusion properties in Fe-Cu alloys. First, we investigate the vacancy migration in dilute Fe-Cu alloys using a static approach and an EAM potential. Then, we discuss how the results can be used in a simple rigid lattice model for vacancy migration.

1. Atomistic kinetic model

From the theory of rate processes (e.g., Ref. 23 and references therein), the jump frequency of an i atom (i=Fe or Cu) on a neighboring vacancy V is given by

$$\Gamma_{i\text{-}V} = \nu_i \exp\left(-\frac{\Delta E^{act}_{i\text{-}V}}{kT} \right), \tag{2.3}$$

where $\Delta E^{act}_{i\text{-}V} = E_{sp} - E_{ini}$ is the activation barrier of the jump (i.e., the energy of system at the saddle point, E_{sp}, minus its initial energy E_{ini}) and where ν_i is the attempt frequency:

$$\nu_i = \prod_{k=1}^{3N} \nu_k^{ini} \Big/ \prod_{k=1}^{3N-1} \nu_k^{sp}, \tag{2.4}$$

where ν_k^{ini} are the $3N$ normal modes in the initial (stable) position and ν_k^{sp} are the $3N-1$ modes in the SP position.

The complete description of the Cu and Fe diffusion properties in the alloy is rather complex since both the activation barriers and the attempt frequencies depend on the local atomic configuration around the i-V pair. When the configurational energy of the alloy is estimated by a sum of pair interactions ϵ_{ij} between atoms and vacancies on a rigid lattice, the activation barrier can be written

$$\Delta E^{act}_{i\text{-}V} = e_i^{sp} - \sum_j \epsilon_{ij} - \sum_{j \neq i} \epsilon_{Vj}, \tag{2.5}$$

where the summations correspond to the bonds which are broken during the jump and where e_i^{sp} is the binding energy of the atom i at the saddle-point position. In the following section e_i^{sp} will be estimated from the EAM potential. The attempt frequency ν_i could also be computed from the EAM potential and Eq. (2.4) (see Ref. 24). However, the jump frequencies are much more sensitive to the variation of $\Delta E^{act}_{i\text{-}V}$ (which is involved in an exponential term) especially at low temperature: in the following, ν_{Fe} and ν_{Cu} are assumed constant and are adjusted on the preexponential factors of the Fe self-diffusion[29] and of the Cu impurity diffusion[22] coefficients in α-iron (see Sec. III A).

2. Comparison with the EAM potential

The aim of this subsection is to test the previous assumptions in dilute $Fe_{1-x}Cu_x$ alloys, using the EAM potential.[16]

a. Computational procedure. We have simulated the migration of a vacancy in the Fe-Cu alloy in a cubic simulation box containing 2000 or 5488 atoms. At first, we have obtained the initial configuration of the alloy using the procedure detailed in Sec. II A 1: the Fe and Cu atoms are placed on a perfect bcc lattice, and the configuration is relaxed using a conjugate gradient algorithm allowing simultaneously the movement of atoms and an isotropic dilatation of the box.

Then, we have set the lattice parameter to the value obtained by the above relaxation and we have used fixed boundary conditions. We have simulated the vacancy migration using the usual static technique. The intermediate atomic positions during the vacancy migration are obtained by linearly interpolating between the initial and final positions and by allowing a relaxation perpendicular to the global jump direction (drag method[25,26]). The accuracy of this method depends on the number of ''relaxed intermediate configurations.'' We have used at least 20 such configurations, and the excess energy $\Delta E^{act}_{i\text{-}V}$ was computed using the maximum en-

TABLE III. Prediction of the EAM potential (Ref. 16) for the activation energies of the jumps frequencies defined in Fig. 2 (first row) and corresponding saddle-point binding energies (second row).

	Γ_0	Γ_2	Γ_3	Γ_3'	Γ_3''	Γ_4	Γ_4'	Γ_4''	Γ_5
ΔE (eV)	0.67	0.225	0.92	0.65	0.65	0.70	0.46	0.46	0.67
e^{sp} (eV)	-9.47	-8.86	-9.25	-9.50	-9.54	-9.28	-9.52	-9.53	−9.49

ergy between 100 linearly interpolated configurations between the relaxed intermediate configurations. We have checked that the accuracy of this procedure on the excess energy $\Delta E_{i\text{-}V}^{act}$ is better than 10^{-3} eV.

Finally, we have obtained the SP binding energies e_i^{sp} with Eq. (2.5) by reintroducing the energy increases $\Delta E_{i\text{-}V}^{act}$ predicted by the EAM potential and the first-nearest-neighbor interaction energies listed in Table II.

b. Nature of the jumping atom. Our first goal was to assess whether (in dilute Fe_xCu_{1-x} alloys) the saddle-point binding energies e_i^{sp} significantly depend on the nature of the jumping atom (i=Fe or Cu). To do so, we have compared, in a pure α-Fe matrix, the jump of a Fe atom with that of an isolated Cu impurity. Using the above procedure and the EAM potential,[16] we have obtained the energy increases $\Delta E_{Fe\text{-}V}^{act}=0.667$ eV and $\Delta E_{Cu\text{-}V}^{act}=0.225$ eV. Reintroducing these values in Eq. (2.5) gives the SP binding energies $e_{Fe}^{sp}=-9.50$ eV and $e_{Cu}^{sp}=-8.88$ eV for a jumping Fe and Cu atom in a α-Fe crystal. Therefore, the SP binding energy significantly depends on the nature of jumping atom.

c. Influence of the local environment. Our second objective was to evaluate the influence of the local atomic configuration surrounding the SP position on the values of e_{Fe}^{sp} and e_{Cu}^{sp}. In the bcc crystals, the SP has six nearest-neighbors positions [see Fig. 2(b)], which are significantly closer (about 30%) than the second-nearest-neighbor ones. Therefore, the atom at the SP is expected to interact more strongly with its first nearest neighbors than with any other atoms.

(i) *Iron SP binding energy*. At first, we have introduced only one Cu impurity in the simulation box and computed the energy increases corresponding to various vacancy exchanges with Fe atoms in the vicinity of the Cu atom with the corresponding jump frequencies $\Gamma_3,\Gamma_3',\ldots,\Gamma_5$ defined in Fig. 2 (according to the notation of Le Claire[27]). The results are summarized in Table III. Reintroducing these values in Eq. (2.5) gives the iron SP binding energies listed in the last row of Table III. These results show that for the jumps Γ_3', Γ_3'', Γ_4', Γ_4'', and Γ_5 the value of e_{Fe}^{sp} is very close to the one obtained in pure α-Fe matrix ($e_{Fe}^{sp}\simeq-9.5$ eV). Indeed, the energy difference is lower than 0.05 eV. We can therefore conclude that these jumps are not significantly modified by the presence of the Cu impurity. However, the iron SP binding energies corresponding to the jumps Γ_3 and Γ_4 are much smaller (by about 0.25 eV, with, respectively, $e_{Fe}^{sp}=-9.25$ eV and -9.28 eV). As shown in Fig. 2, these two jumps correspond to a case where the Cu impurity is in a first-nearest-neighbor position of the saddle point. Therefore, when computing the SP binding energy, it seems that the influence of the Cu impurity can indeed be neglected unless the impurity is in a first-nearest-neighbor position of the saddle point.

Then, we have considered more than 30 different jumps of a Fe atom where we have varied the number and position of the surrounding Cu atoms. We have introduced up to six Cu impurities. Using the above procedure, we have found e_{Fe}^{sp} ranging from -9.50 eV to -7.97 eV for the jump of an Fe atom. Therefore, the iron SP binding energy is extremely sensitive to the surrounding Cu impurities. We have found the minimum value in the absence of Cu impurity and the maximum value when six Cu impurities are introduced in the six first nearest positions of the SP.

For that reason, we have sorted all the e_{Fe}^{sp} values that we have obtained for a jumping Fe atom with respect to the number of first nearest-neighbor Cu impurities. The result, presented in Table IV, shows clearly that the iron SP binding energy is mainly a function of the nature of the first nearest neighbors of the atom at the saddle point (NNSP). Even if the limited number of jumps considered here is not sufficient to get a good statistics, the mean deviation obtained for e_{Fe}^{sp} (with the same number of NNSP Cu atoms) is very low (less than 0.04 eV).

In other words, we have shown that the iron SP binding energy is sensitive to the number of Cu atoms in the nearest-neighbor sites of the SP, but is not sensitive to their position inside the six possible neighbor sites of the SP. Moreover, the e_{Fe}^{sp} values given in Table III increase linearly with the number of NNSP Cu atom. This result means that the iron SP binding energy can be described by a simple pair interaction model between the atom at the SP position and its six first nearest neighbors i:

$$e_{Fe}^{sp}=\sum_i \epsilon_{Fe*i}^{sp}, \tag{2.6}$$

where $Fe*$ designates the Fe atom at the SP position. For each jump, we have computed the interaction energies ϵ_{Fe*Fe}^{sp} and ϵ_{Fe*Cu}^{sp}. In the following Monte Carlo (MC) simulations, we use the mean values (over all the Fe jumps

TABLE IV. Saddle-point binding energy (e_{Fe}^{sp}) of a Fe atom as a function of the number of Cu atoms in a first-nearest-neighbor position and its mean deviation σ.

NNSP Cu	0	1	2	3	4	5	6
e_{Fe}^{sp} (eV)	-9.50	-9.29	-9.05	-8.84	-8.59	-8.31	-7.97
σ (eV)	0.03	0.03	0.02	0.04	0.02	-	-

we have computed) obtained by this procedure: $\epsilon^{sp}_{Fe*Fe} = -1.583$ eV and $\epsilon^{sp}_{Fe*Cu} = -1.345$ eV.

(ii) *Copper SP binding energy*. We have done a similar analysis for a jumping Cu atom: we have considered configurations containing up to six Cu impurities surrounding the jumping Cu atom. We have found that the copper SP binding energy is much less sensitive to the nature of the surrounding atoms. Indeed, in our calculations e^{sp}_{Cu} is always close to the value -8.86 eV obtained for the isolated Cu impurity. The maximum deviation that we have observed is 0.17 eV ($e^{sp}_{Cu} = -9.01$ eV) when the jumping Cu atom is surrounded by three Cu impurities located in the first-nearest-neighbor positions labeled 1, 2, and 3 in Fig. 2(b). Thus the energy variation in the case of a jumping Cu atom is one order of magnitude lower than the one observed for a jumping Fe atom.

In other words, as a first approximation, we can consider that e^{sp}_{Cu} is not a function of the number of the surrounding Cu impurities. This point is best illustrated by the jump of a Cu atom surrounded by six Cu impurities occupying the six nearest-neighbor positions of the SP. The relaxation of the EAM potential gives an energy increase $\Delta E^{act}_{Cu\text{-}V} = 0.465$ eV. Using Eq. (2.5), one obtains the saddle-point binding energy $e^{sp}_{Cu} = -8.86$ eV which is equal to the value obtained for an isolated jumping Cu atom.

We thus conclude that, compared with the case of jumping Fe atom, the copper SP energy of jumping Cu atom does not significantly depend on the nature of the surrounding atoms. In the following MC simulations, we use the value $e^{sp}_{Cu} = -8.88$ eV which is the mean value of all the copper SP binding energies that we have computed. This is equivalent to saying that the nearest-neighbor interaction energies of the Cu atom at the SP position with Cu and Fe atoms are the same: $\epsilon^{sp}_{Cu*Fe} = \epsilon^{sp}_{Cu*Cu} = -1.480$ eV

Note that, because the SP positions are not equivalent to the stable lattice positions, the pair interaction energies are not symmetrical (i.e., $\epsilon^{sp}_{Cu*Fe} \neq \epsilon^{sp}_{Fe*Cu}$).

C. Monte Carlo method

1. Residence time algorithm

In order to study the diffusion properties and the precipitation kinetics in Fe-Cu alloys, the above atomistic diffusion model on a rigid lattice and its pair interaction parameters derived from the EAM potential can be handled by MC simulations. We consider dilute $Fe_{1-x}Cu_x$ alloys on a rigid bcc lattice with $N = L^3$ sites, periodic boundary conditions, N_{Fe} iron atoms, N_{Cu} copper atoms, and N_V vacancies ($N_{Fe} + N_{Cu} + N_V = N$). In all the following simulations, we use $N_V = 1$, i.e., one vacancy in the simulation box.

As in the previous sections, diffusion occurs by vacancy exchanges with nearest-neighbor atoms. The corresponding jump frequencies $\Gamma_{i\text{-}V}$ are given by Eqs. (2.3) and (2.5). At each Monte Carlo Step (MCS), one of the Z possible vacancy jumps is chosen according to the residence time algorithm described in previous papers.[8,15,28] The probability for a given configuration to be destroyed by one specific vacancy jump towards the atom i is $\Gamma_{i\text{-}V}/\Sigma^{Z}_{j=1}\Gamma_{j\text{-}V}$, where j labels the Z nearest neighbors around the vacancy. The mean lifetime of the configuration, i.e., the physical time of the corresponding Monte Carlo step, is given by

$$t_{MCS} = 1 \Big/ \left(\sum_{i=1}^{Z} \Gamma_{i\text{-}V} \right). \tag{2.7}$$

Therefore a kinetic pathway is defined by (i) the sequence of configurations the system goes through and (ii) the time at which the system reaches each of these configurations.

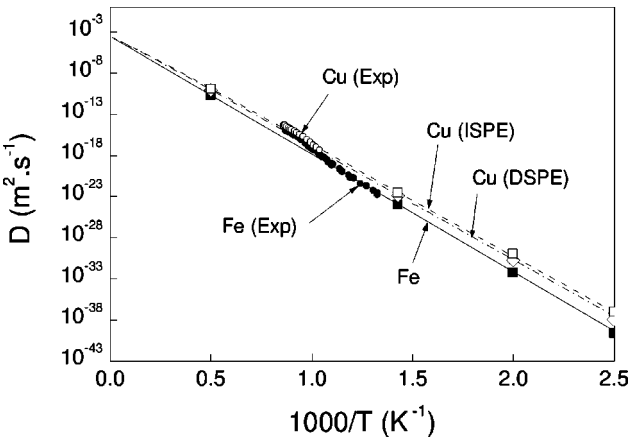

FIG. 3. Arrhenius plot of the iron self-diffusion coefficient D^{Fe}_{Fe*} and of the copper impurity diffusion coefficient D^{Fe}_{Cu*} in α-iron. The circles correspond to the experimental values of D^{Fe}_{Fe*} compiled in Ref. 29 (●) and of D^{Fe}_{Cu*} given by Salje and Feller-Kniepmeier (Ref. 22) (○). The lines correspond to the value of predicted by the theory of diffusion for D^{Fe}_{Fe*} [Eq. (3.1), solid line] and D^{Fe}_{Cu*} [Eq. (3.2), dashed line with the ISPE parameters and dot-dashed line with the DSPE parameters]. The squares and lozenges correspond to the values measured in Monte Carlo simulations for D^{Fe}_{Fe*} (■) and D^{Fe}_{Cu*} (◇ with DSPE, □ with IPSE parameters).

2. Absolute time scale

The diffusion properties and the precipitation kinetic pathway depend on the jump frequencies [Eq. (2.3)] but also on the vacancy concentration. Therefore, to relate the physical time to the time obtained in our Monte Carlo simulations, we have to take into account that the vacancy concentration in the simulation box is usually much more important than the experimental one. Under the usual assumption that the vacancy-vacancy interaction can be neglected, the physical time t_S related to one Monte Carlo step is

$$t_S = t_{MCS} \frac{C^{MC}_V(\mathrm{Fe})}{C^{expt}_V(\mathrm{Fe})}, \tag{2.8}$$

where $C^{expt}_V(\mathrm{Fe})$ and $C^{MC}_V(\mathrm{Fe})$ are the vacancy concentration in the Fe matrix for a real alloy and in a simulation box.

During isothermal aging, we may assume that the vacancy concentration in the Fe matrix is always close to the equilibrium one, so that

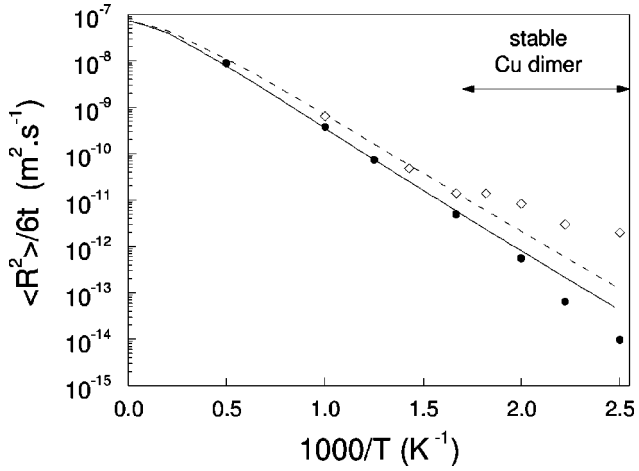

FIG. 4. Diffusion coefficients of a 2-Cu cluster (at constant vacancy concentration $C_V = 1/16^3$) measured in MC simulations with DSPE (●) and ISPE (◇) parameters. The lines correspond to the diffusion coefficient of Cu monomers (for the same vacancy concentration) with DPSE (solid line) and ISPE (dashed line) parameters.

$$C_V^{expt}(\mathrm{Fe}) \simeq C_V^{eq}(\mathrm{Fe}) = \exp\left[-\frac{E_V^{for}(\mathrm{Fe})}{kT}\right], \qquad (2.9)$$

where $E_V^{for}(\mathrm{Fe})$ is the vacancy formation energy in pure iron [Eq. (2.2)]. Indeed, even when vacancies are trapped inside precipitates (as is the case in Fe-Cu alloys), vacancy sources (grain boundaries, dislocation, etc.) act to maintain the vacancy concentration in the matrix close to the equilibrium one. In other words, we assume that the microstructure in Fe-Cu alloys evolves slowly compared with the characteristic time for the creation of a vacancy by a source.

In our simulation box, we introduce only one vacancy. The average vacancy concentration in the simulation box is then simply $\overline{C_V} = 1/L^3$. However, the vacancy concentration in the iron matrix $C_V^{MC}(\mathrm{Fe})$ highly depends on the trapping of the vacancy by the copper precipitates and evolves during the microstructure evolution (see below, Sec. IV A, and Fig. 8). To take this effect into account, we measure the fraction of time spent by the vacancy in the iron matrix $f_V^{MC}(\mathrm{Fe})$ and compute the vacancy concentration by

$$C_V^{MC}(\mathrm{Fe}) = f_V^{MC}(\mathrm{Fe})/(X_{Fe}^{vol} \times L^3), \qquad (2.10)$$

where $X_{Fe}^{vol} \simeq 1$ is the iron matrix volume fraction. The vacancy is considered in the iron matrix when there is no Cu atoms among its $Z=8$ nearest neighbors. Typically, for a simulation of 10^{11} MCS (10^{11} MCS vacancy jumps) a mean value of $f_V^{MC}(\mathrm{Fe})$ is computed every 10^4 MCS at the beginning of the decomposition (when the precipitates microstructure evolves rapidly). At the end it can be computed over typically 10^8 MCS. If no significant vacancy trapping occurs, as is the case with the parameters of the previous studies of Refs. 7 and 15, this expression simply gives $C_V^{MC}(Fe) = 1/L^3$.

TABLE V. Interaction energies between an atom at the saddle-point position and its first nearest neighbors (in eV). The first row (DSPE) corresponds to the interaction energies fitted to reproduce the EAM results. The second row (ISPE) contains the interaction energies used in the simulations where the SP binding energy is independent of the local environment (see text for explanations).

	ϵ_{Fe*Fe}^{sp}	ϵ_{Fe*Cu}^{sp}	ϵ_{Cu*Cu}^{sp}	ϵ_{Cu*Fe}^{sp}
DSPE	-1.583	-1.345	-1.480	-1.480
ISPE	-1.583	-1.583	-1.480	-1.480

Finally, the physical time during a Monte Carlo simulation is obtained by summing the time increments t_S [Eq. (2.8)] where the vacancy concentrations are obtained with Eqs. (2.9) and (2.10).

3. DSPE and ISPE sets of parameters

To compute the jumps frequencies $\Gamma_{i\text{-}V}$, we have used the parameters given in Table V. The attempt frequencies ν_{Fe} and ν_{Cu} have been fitted to the preexponential factor of the Fe and Cu diffusion coefficients in pure iron (see Sec. III). The values are approximatively the same for Fe and Cu: $\nu_i \simeq 5 \times 10^{15}$ s^{-1}.

We have paid special attention to the strong dependence of e_{Fe}^{sp} on the local atomic configuration, since previous MC studies have indeed shown that the kinetic pathway of phase transformations may depend on such details of the jump frequencies.[7,8] In the following, we use two sets of MC parameters. Both use the first-nearest-neighbor pair interaction energies (ϵ_{ij}) derived from the EAM potential for the configurational energies (see Table II). However, the two sets of parameters differ by the value of the interaction energies between an atom at the SP position and its first nearest neighbors (ϵ_{i*j}^{sp}).

(i) In the first set, the SP pair interaction energies ϵ_{i*j}^{sp} are those previously derived from the EAM potential and recalled in the first row of Table V. Therefore the SP binding energy depends both on the nature of the jumping atom and on that of the nearest neighbors of the SP. It will be referred to as the DSPE (dependent saddle-point binding energy).

(ii) We have constructed another set of parameters which gives the same SP binding energies than the first set in the case of a jumping Fe atom and in the case of a jumping isolated Cu impurity in a pure α-Fe matrix. However, in this set, e_{Fe}^{sp} and e_{Cu}^{sp} are constants ($e_{Fe}^{sp} = -9.50$ eV and $e_{Cu}^{sp} = -8.88$ eV); i.e., they do not depend on the nature of the surrounding atoms. In other words, the two sets only differ by the value of ϵ_{Fe*Cu}^{sp}: we impose here $\epsilon_{Fe*Cu}^{sp} = \epsilon_{Fe*Fe}^{sp} = -1.583$ eV. This set will be referred to as the ISPE (independent saddle-point binding energy), because this set does not take into account the influence of the surrounding atoms on the value of e_{Fe}^{sp} and e_{Cu}^{sp}.

Note that the two sets of parameters correspond to the same equilibrium properties (phase diagram, interfacial energy, vacancy formation energy, etc.) and to the same Fe self-diffusion coefficient, but as we will see in the following

section, the difference in e_{Fe}^{sp} sightly affects the Cu impurity diffusion coefficient and greatly modifies the mobility of small Cu clusters.

III. DIFFUSION IN DILUTE Fe-Cu ALLOYS

The diffusion properties of our Fe-Cu model system on rigid lattice, with the parameters of Table V derived from the EAM potential, can be discussed using both the atomic theory of diffusion (e.g., Ref. 23) and Monte Carlo simulations. The first method gives analytical expressions of the Fe self-diffusion and Cu impurity diffusion coefficients as a function of a few jump frequencies given by Eq. (2.3). These expressions are then compared with a direct measurement by MC simulation. The small Cu clusters may also have some mobility, depending on the details of the jump frequencies parameters:[7] the MC method gives a measurement of the corresponding diffusion coefficients.

A. Self-diffusion and solute diffusion

The self-diffusion coefficient in an α-Fe crystal is given by[23]

$$D_{Fe*}^{Fe}=a^2\Gamma_0 f_0 C_V^{eq}(\mathrm{Fe}), \tag{3.1}$$

where $a=0.287$ nm is the iron lattice parameter, Γ_0 the Fe-V exchange frequency in pure iron and f_0 the autodiffusion correlation factor ($f_0\simeq 0.727$ in the bcc structure).

The diffusion coefficient of a Cu impurity in pure α-Fe is given by[27]

$$D_{Cu*}^{Fe}=a^2\Gamma_2 f_2 \frac{\Gamma_4'}{\Gamma_3'} C_V^{eq}(\mathrm{Fe}) = a^2\Gamma_2 f_2 \exp\left[-\frac{E_V^{\mathrm{for}}(\mathrm{Fe})+E_{V\text{-}Cu}^{b}(1)}{kT}\right], \tag{3.2}$$

where Γ_2 is the rate of vacancy-Cu jumps in pure iron, and f_2 is the impurity correlation factor. Contrary to the case of self-diffusion, f_2 is not a geometric factor, but depends on the atomic jump frequencies of the vacancies and, then, on the temperature. To evaluate f_2 for a Cu impurity, we consider the nine-frequency model developed by Le Claire[27] for the heterodiffusion in a bcc crystal. In this model, three distinct dissociative frequencies are defined for a vacancy escaping from the first-neighbor shell of the Cu impurity: the vacancy dissociation jumps can occur from first to second, third, and fifth neighbors with jump rates Γ_3, Γ_3', and Γ_3'', respectively. The corresponding reverse association jumps occur with rates Γ_4, Γ_4', and Γ_4'' (see Fig. 2 for notation). Second nearest neighbors are sufficiently close in that the rate of dissociation jumps from them to fourth neighbors may be affected by the Cu atom, so we distinguish them by the rate Γ_5. We assume that all other jumps occur at the solvent rate Γ_0. Under these assumptions, the impurity correlation factor $f_2=(1+t_1)/(1-t_1)$ is given by[27]

$$t_1=\frac{-\Gamma_2}{\Gamma_2+3\Gamma_3+3\Gamma_3'+\Gamma_3''-\dfrac{\Gamma_3\Gamma_4}{\Gamma_4+F\Gamma_5}-\dfrac{2\Gamma_3'\Gamma_4'}{\Gamma_4'+3F\Gamma_0}-\dfrac{\Gamma_3''\Gamma_4''}{\Gamma_4''+7F\Gamma_0}}, \tag{3.3}$$

where $F=0.512$.

Note that the calculation of the correlation factor is usually not performed with the whole set of frequencies. The two simplifying assumptions used in the literature[23] are "model I" where $\Gamma_4=\Gamma_4'=\Gamma_0$ and "model II" where $\Gamma_3'=\Gamma_3''=\Gamma_3, \Gamma_5=0$, and the interactions are restricted to first neighbor distances.

The computation of the Cu diffusion coefficient (3.2) requires knowledge of the jump frequencies $\Gamma_0,\ldots,\Gamma_5$. We have used our static approach with the EAM potential to compute the activation energies of these jump frequencies. In the following, the attempt frequency is assumed constant for all jumps. The results are presented in Table III: it is clear that the simplifying assumptions for model I and model II do not apply in the Fe-Cu system. However, the results suggest a new assumption ("model III") defined by the equations $\Gamma_5=\Gamma_0$, $\Gamma_3'=\Gamma_3''$, and $\Gamma_4'=\Gamma_4''$ and where the interactions are restricted to first-neighbor distances. This model is less restrictive than the model II where, in addition, $\Gamma_3=\Gamma_3'$. Most interestingly, the assumption of a first-nearest-neighbor interaction scheme, both for the configurational energy and for the saddle-point binding energy, necessarily implies the conditions of model III. However, the additional condition for model II is not fulfilled because the energy increases ΔE_3 and $\Delta E_3'$ corresponding to the jump frequencies Γ_3 and Γ_3' are different:

$$\Delta E_3-\Delta E_3'=\epsilon_{Fe*Fe}^{sp}-\epsilon_{Fe*Cu}^{sp}.$$

The above equation shows clearly that model II does not apply for Fe-Cu alloys because the iron SP binding energy depends on the local environment.

We have introduced the jump frequencies given in Tables III and IV in the analytical solution of the Le Claire model. It gives an activation energy close to $E_a(f_2)=0.47$ eV for the correlation factor between 500 K and 1500 K. The large value of this activation energy reflects the high correlation effects between successive Cu-V exchanges: each exchange is almost always immediately followed by the reverse one

(because of the small value of the ΔE_2 activation barrier). This strongly decreases the efficiency of Cu impurity diffusion at low temperature.

Finally, the activation energy of the Fe self-diffusion coefficient predicted by the EAM potential[16] is [Eq. (3.1)] $E_a(D^{Fe}_{Fe*})=E^{for}_V+\Delta E_0=2.3$ eV. For the Cu impurity diffusion coefficient [Eq. (3.2)] it is $E_a(D^{Fe}_{Cu*})=E_a(f_2)+E^{for}_V+E^b_{V\text{-}Cu}(1)+E_a(\Gamma_2)=2.1$ eV. It predicts a faster diffusion of Cu impurities than the Fe self-diffusion, as is experimentally observed. However, in order to reproduce quantitatively the experimental values of the preexponential factors and the activation energies of the Fe self-diffusion and the Cu impurity diffusion coefficients, we have to choose the attemps frequencies $\nu_{Fe}=\nu_{Cu}=5\times10^{15}$ s^{-1} and to increase both the Cu and Fe activation barriers by the same value 0.6 eV. This discrepancy of 0.6 eV between the experiemental and computed activation barriers is due to the low vacancy migration energy predicted by the EAM potential. Indeed, in pure α-Fe, the vacancy migration energy predicted by the EAM potential is 0.67 eV whereas the experimental measurements are close to 1.2 eV.[29] Note that the pseudopotential approach by Osetsky *et al.*[18] and the EAM potential developed by Ackland *et al.*[17] also give very low vacancy migration energies in α-Fe (0.53 eV and 0.78 eV, respectively).

B. Diffusion coefficients measured by Monte Carlo simulations

The Fe self-diffusion and Cu impurity diffusion coefficients have been also directly measured in the Monte Carlo simulation from the mean-square displacement $\langle R_i^2\rangle$ of each i atom:[23] $D^{Fe}_{i*}=\langle R_i^2\rangle/(6t)$. In order to compare this measurement and the predictions of model III with experimental data, two kinds of corrections have to be done.

(i) As explained above, the migration energies of both Cu and Fe given by the EAM potential[16] are too small by approximatively the same 0.6 eV quantity: the time is then rescaled, both in the MC simulations and in model III, by a factor $\exp[+0.6(\mathrm{eV})/kT]$ (this can be viewed as increasing each $\epsilon^{sp}_{i*_j}$ parameter by the same 0.1 eV quantity: all the possible jump frequencies are changed by the same factor, so that kinetic pathway remains is the same, except for a time rescaling by a *constant* factor).

(ii) Since we use only one vacancy in the simulation box, the time is also rescaled in the MC simulations, as explained in Sec. II C 2, to take into account the temperature dependence of C_V in the iron matrix.

Taking these corrections into account, Fig. 3 displays the experimental values of D^{Fe}_{Fe*} (from Ref. 29) and D^{Fe}_{Cu*} (from Ref. 22); the theoretical values computed with ''model III'' [Eqs. (3.1) and (3.2)] with the two sets of parameters DSPE and ISPE, the values measured by MC simulations, again with the DSPE and ISPE sets of parameters.

As can be seen, there is a good general agreement between the different methods. The diffusion of Cu impurities in iron is slightly faster than the iron self-diffusion. The iron and the copper diffusion coefficients measured in the Monte Carlo simulations are very close to the values computed with ''model III,'' both with DSPE and ISPE parameters: the Cu impurity diffusion coefficient is slightly smaller when the dependence of the Fe saddle-point energy is taken into account, and the difference decreases slowly with increasing temperatures [e.g., $D^{Fe}_{Cu*}(\mathrm{ISPE})/D^{Fe}_{Cu*}(\mathrm{DSPE})\simeq3$ at 500 K and $\simeq2$ at 1000 K]. This is due to the influence of the Cu impurity on the e^{sp}_{Fe} parameters involved in the two jump frequencies Γ_3 and Γ_4 (see Fig. 2), which leads to a decrease of the correlation factor f_2 [see Eq. (3.2)]. However, the difference is quite small when compared with the accuracy of the experimental measurements.

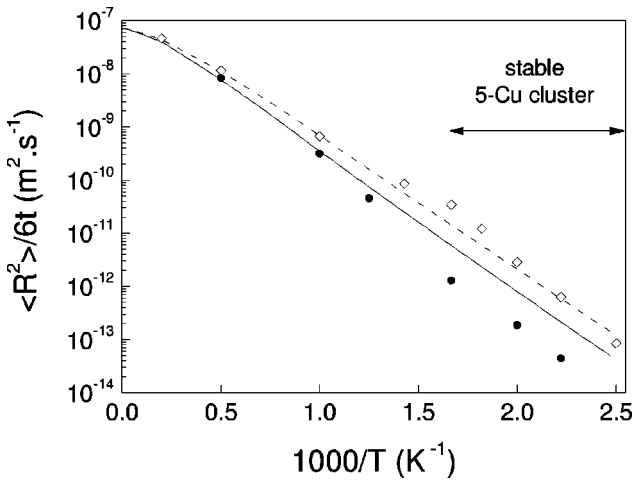

FIG. 5. Diffusion coefficients of a 5-Cu cluster (at constant vacancy concentration $C_V=1/16^3$) measured in MC simulations with DSPE (●) and ISPE (◇) parameters. The lines correspond to the diffusion coefficient of Cu monomers (for the same vacancy concentration) with DPSE (solid line) and ISPE (dashed line) parameters.

Because of the very strong dependence of these diffusion coefficients with the temperature, it is also clear that these relatively small differences are difficult to illustrate in a figure such as Fig. 3: in the following, we will compare the diffusion coefficients obtained with DSPE and ISPE parameters at constant $\overline{C_V}$ (typically $\overline{C_V}=1/16^3$).

C. Copper cluster diffusion coefficients

The diffusion coefficient of small Cu clusters can be measured at low temperature in the MC simulations using the following procedure. A small cluster of n Cu atoms is initially introduced in a pure iron simulation box with one vacancy. At low temperature the Cu cluster is stable (no emission of Cu monomer is observed) and the cluster has to migrate as a whole: The cluster diffusion coefficient $D^{Fe}_{n\text{-}Cu}$ is then directly given by the average of $\langle R^2_{Cu}\rangle/(6t)$ on the n Cu atoms. Note that this method cannot be applied at high temperature, because the clusters dissociate into smaller clusters or individual Cu atoms.

The values of $\langle R^2_{Cu}\rangle/(6t)$ measured for a Cu dimer and for a 5-Cu cluster are displayed in Figs. 4 and 5. In both cases, the clusters are stable when $T<600$ K. Between 600 and 800 K, they are sometimes dissociated (the 5-Cu clusters is often dissociated into one or two 2-Cu clusters and Cu

monomers), while for $T>1000$ K the Cu clusters are almost completely dissociated into monomers. As a consequence, in the latter case ($1000/T<1$ in Figs. 4 and 5), the measurements of $\langle R^2_{Cu}\rangle/(6t)$ give almost the values of the Cu impurity diffusion coefficient in iron.

At first, we have found that the mobility of small Cu clusters is significant when compared with the impurity diffusion coefficient. As shown in Figs. 4 and 5, we have observed this behavior with both sets of parameter (ISPE and DSPE). This point is in agreement with a previous work[15] where the mobility of small Cu clusters was already noticed. As we will see below, this mobility is explained by a strong vacancy trapping on the Cu precipitates.

Second, we have found that the two sets of parameters differ when quantitatively comparing the mobilities of small clusters with that of Cu impurities. This point is rather clear in Fig. 4 where it is shown that, with the DSPE set, the dimers migrate more slowly than the monomers, whereas the opposite is true when using the ISPE set:

$$\frac{D^{Fe}_{2\text{-}Cu}(\text{DSPE})}{D^{Fe}_{Cu*}(\text{DSPE})} \ll 1 \ll \frac{D^{Fe}_{2\text{-}Cu}(\text{ISPE})}{D^{Fe}_{Cu*}(\text{ISPE})}.$$

The same trend is observed for the diffusion coefficients of clusters containing five Cu atoms (Fig. 5): With the ISPE set, 5-mers have about the same mobility than individual Cu atoms. However, the 5-mers diffuse about 8 times slower than the monomers with the DSPE set.

Finally, as in the case of the Cu impurity diffusion, our simulations show that the small Cu cluster diffusion is reduced when the influence of the local atomic configuration on the SP binding energy is taken into account (see Figs. 4 and 5). This trend is due to the increase of the energy barrier for vacancy migration when Cu atoms are close to the SP position (DSPE set). However, the choice of the set of parameters (ISPE or DSPE) affects more strongly the small Cu clusters diffusion than the Cu impurity diffusion. For example, below 500 K the diffusion coefficient of the Cu dimers is almost two orders of magnitude lower when e^{sp}_{Fe} depends on the local configuration (DSPE set). In the same conditions, the Cu impurities migrate only 2 or 3 times slower.

As a summary, we have shown that, in dilute Fe_xCu_{1-x} alloys, the mobility of small Cu clusters is significant when compared with the impurity diffusion coefficient. Moreover, the Cu clusters are less mobile when the dependence of e^{sp}_{Fe} as a function of the local atomic configuration is taken into account. Finally, at low temperature, details of the diffusion mechanism (such as the influence of the SP binding energy on local atomic configuration) have to be taken into account to estimate correctly the mobilities of small Cu clusters.

IV. PRECIPITATION KINETICS

To follow the precipitation kinetics in $Fe_{1-x}Cu_x$ alloys, we use MC simulations with a box of $N=64^3$ lattice sites and one vacancy (i.e., $\overline{C}^{MC}_V \simeq 3.8\times10^{-6}$). The precipitation process is detailed in Figs. 6 and 7 for two compositions and temperatures (in Fig. 6, T=1000 K and $x=1\%$, and in Fig. 7, $T=573$ K and $x=3\%$). The microstructural evolution is characterized by three quantities: the short-range order α_{Cu} around Cu atoms (α_{Cu} is the averaged fraction of Cu atoms among the Z first neighbors of Cu atoms), the number $N_p(i>i^*)$ of precipitates larger than the critical size, and their average size $\langle i\rangle$.[38]

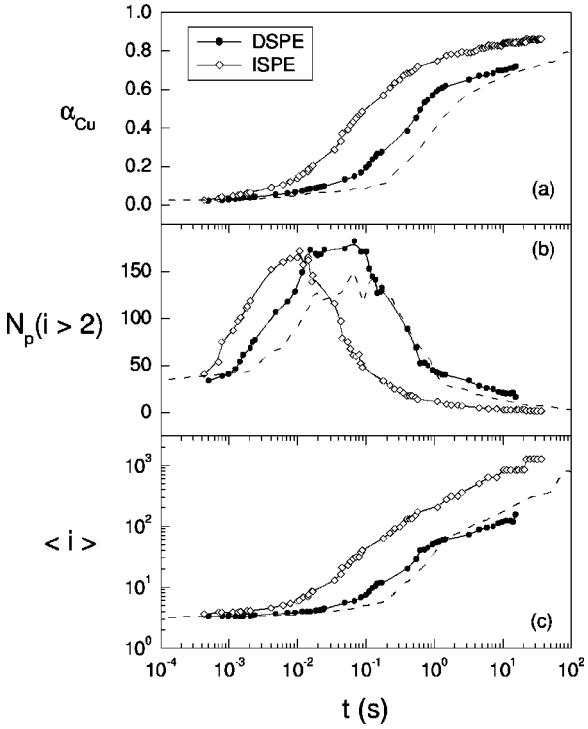

FIG. 6. Precipitation kinetics in a $Fe_{0.99}Cu_{0.01}$ alloy at $T=1000$ K: time evolution of (a) the degree of short-range order α_{Cu}, (b) the number of supercritical precipitates N_p ($i>i^*$), and (c) the averaged size of supercritical precipitates $\langle i\rangle$. Monte Carlo simulations with DSPE (●) and ISPE (◇) parameters. The dashed lines correspond to the kinetics observed with the parameters of Ref. 15 (see Appendix).

A. High temperature: $T=1000$ K, $x=1\%$

The evolution, as a function of the number of MCS, of the fraction of time f^{MC}_V(Fe) spent by the vacancy in pure iron (i.e., with $Z=8$ iron atoms as first neighbors), is given in Fig. 8. During the first 10^7 MCS, it is almost constant [$(f^{MC}_V(\text{Fe})\sim0.6$]; i.e., the vacancy spends 55% of its time in pure iron. This plateau corresponds to the nucleation stage. Then, as the growth regime starts, the vacancy trapping at the Fe-Cu interfaces and in the Cu precipitates becomes more effective and f^{MC}_V(Fe) decreases rapidly. At the end of the simulation the trapping effect is quite important, since f^{MC}_V(Fe) reaches 4×10^{-2} for the ISPE set and 7×10^{-2} for the DSPE set. These values are still slightly above the expected value for a complete precipitation [$f^{eq}_V(\text{Fe})\simeq2.3\times10^{-2}$], because of the relatively large fraction of interfacial sites.

The evolutions of f^{MC}_V(Fe) observed with the DSPE and ISPE sets of parameters are very similar, except for a shift in

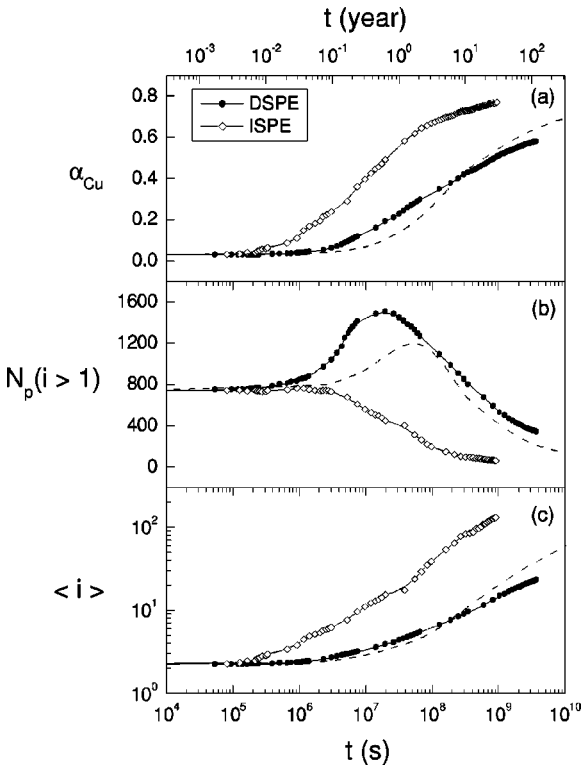

FIG. 7. Precipitation kinetics in a $Fe_{0.97}Cu_{0.03}$ alloy at $T=573$ K: time evolution of (a) the degree of short-range order α_{Cu}, (b) the number of supercritical precipitates N_p $(i>i^*)$, and (c) the averaged size of supercritical precipitates $\langle i \rangle$. Monte Carlo simulation with DSPE (●) and ISPE (◇) parameters. The dashed lines correspond to the kinetics observed with the parameters of Ref. 15 (see Appendix).

the MCS scale. As previously explained, the physical time is rescaled according to Eq. (2.8) to take into account this vacancy trapping, with the assumption that in a real system the vacancy concentration is always at equilibrium in the iron matrix. It is worth noticing that the equilibrium vacancy concentrations in iron and copper, and so $f_V^{eq}(\mathrm{Fe})$, do not depend on the SP binding energies e_{Fe}^{sp} and e_{Cu}^{sp}, so that it is the same for the ISPE and DSPE sets of Monte Carlo parameters.

The microstructural evolution is given in Fig. 6. At this temperature the kinetics is quite fast. With the ISPE set of parameters, a nucleation stage can be identified for approximatively $t<10^{-2}$ s: the copper supersaturation (and then the degree of short range order α_{Cu}) is almost constant and the number of Cu precipitates increases rapidly with time, while their average size is almost constant. At longer time, the number of precipitates decreases and their size increases during the growth and coarsening regimes. However, due to the high supersaturation,[15] these two regimes overlap and are difficult to distinguish.

When the dependence of e_{Fe}^{sp} on the local atomic configuration is taken into account, the kinetic is slower than when it is not (Fig. 6). The slowing down factor is almost constant (approximatively one order of magnitude). In the classical theories of precipitation in solid solutions, the kinetics of nucleation, growth, and coarsening are proportional to the

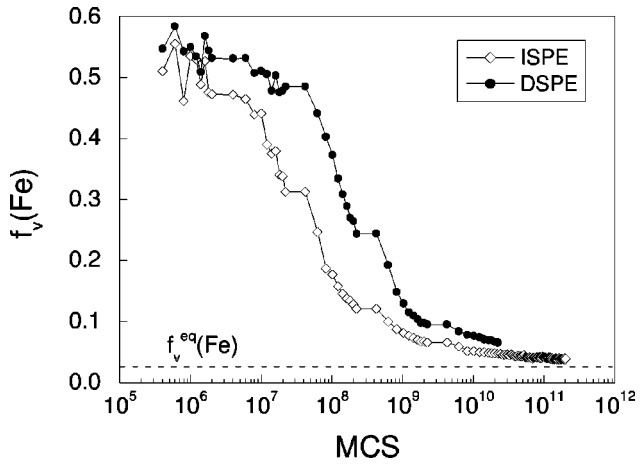

FIG. 8. Evolution of the fraction of time spent by the vacancy in pure iron during a precipitation in a $Fe_{0.99}Cu_{0.01}$ alloy at $T=1000$ K: Monte Carlo simulation with DSPE (solid line) and ISPE (dashed line) parameters.

solute diffusion coefficient. Therefore, because $D_{Cu*}^{Fe}(\mathrm{ISPE}) \simeq 2D_{Cu*}^{Fe}(\mathrm{DSPE})$ at $T=1000$ K, we should expect a kinetic evolution twice slower with the DSPE set of parameters than with the ISPE one. But indeed, taking into account the influence of the surrounding atoms on e_{Fe}^{sp} also modifies the correlation effects between the successive vacancy jumps and therefore the mobility of small Cu clusters (see Sec. III C), their direct coagulation, and their spatial distribution. These effects, which are not taken into account in the classical theories, appear to be very important, since finally the discrepancy between the ISPE and DSPE kinetics is close to one order of magnitude.

B. Low temperature: $T=573$ K, $x=3\%$

At lower temperatures, the influence of the migration energy differences between the two sets of parameters is enhanced and we expect stronger effects on the kinetics pathway. Furthermore, the vacancy trapping inside copper precipitates and at their interface with the iron matrix increases [one measures typically $f_V^{MC}(\mathrm{Fe}) \simeq 1\times 10^{-4}$ at $T=573$ K for the last precipitation steps of Fig. 7]: so as will be discussed below, the direct coagulation between clusters is favored.[6]

At $T=573$ K, the precipitation kinetics is of course much more slowler than at $T=1000$ K (Fig. 7). As in the high-temperature case, the kinetics is faster with the ISPE than with the DSPE set of parameters, and the difference is much greater than expected from the impurity diffusion coefficients $[D_{Cu*}^{Fe}(\mathrm{ISPE})/D_{Cu*}^{Fe}(\mathrm{DSPE}) \simeq 2.5$ at $T=573$ K]. However, the shift observed in Figs. 7(a) and 7(c) is no longer a constant, but increases with time.

Most interestingly, the differences observed in Fig. 7(b) with the two sets of parameters cannot be reduced to a simple shift on the time scale. More precisely, with the DSPE the number of precipitates, $N_p(i>i^*)$, exhibits a clear increase between $t\sim 10^6$ and 10^7 s before a decrease. With the ISPE, this kind of nucleation regime vanishes and N_p $(i$

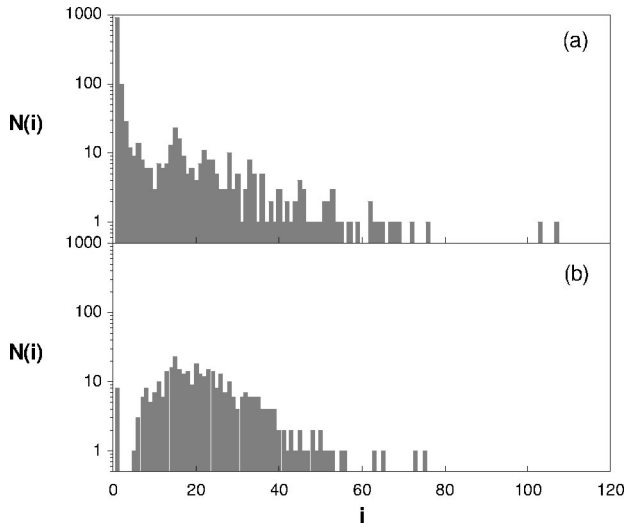

FIG. 9. Precipitation kinetics in a $Fe_{0.97}Cu_{0.03}$ alloy at $T=573$ K: clusters size distributions observed in the Monte Carlo simulations with ISPE (a) and DSPE (b) parameters for the same degree of short-range order $\alpha_{Cu}\simeq 0.6$ and the same mean cluster size $\langle i\rangle \simeq 20$.

$>i^*$) monotically decreases. This different behavior can be related to the diffusion properties of small Cu clusters. During the first precipitation stage, the time evolution of N_p ($i>i^*$) is governed by the balance between direct coagulation of clusters [which results in a decrease of N_p ($i>i^*$)] and the copper monomer adsorption [which, at this stage, results in an increase of N_p ($i>i^*$)]. With the ISPE, small Cu clusters are more mobile (Figs. 4 and 5): the number of precipitates immediatly decreases. With the DSPE, Cu monomers are more rapid than small clusters (Figs. 4 and 5): the number of precipitates grows as long as the matrix contains enough monomers they can adsorb.

Differences between ISPE and DSPE sets of parameters are also observed at longer time: they can be seen for example on the size distribution of copper clusters (Fig. 9). The distributions obtained with the ISPE and DSPE are displayed for a same degree of short-range order ($\alpha_{Cu}\simeq 0.6$) and a same average cluster size ($\langle i\rangle \simeq 20$ copper atoms). The distribution is narrower when the dependence of the SP binding energy is taken into account. Moreover, since this short-ordering state is reached after a longer annealing time ($t\simeq 3\times 10^9$ s with DSPE vs $t\simeq 4\times 10^7$ s with ISPE), the number of Cu monomers is then smaller than with the ISPE set of parameters. Athènes *et al.*[28] have already noticed that cluster size distributions are broader when small solute clusters are mobile, i.e., when the direct coagulation between precipitates is the dominant growth process.

These differences can also modify the kinetics of latter precipitation stages, such as the beginning of the coarsening stage, since when the distribution is broad, a lot of small precipitates can shrink to the benefit of larger ones, while when it is narrow, the competition between precipitates of similar size is harder. This could explain the lower growth exponent observed with DSPE, for the latest times of Fig. 7(c).

V. DISCUSSION AND CONCLUSION

We have used both an EAM potential and a diffusion model on rigid lattice to simulate the coherent precipitation of Cu in α-iron by the Monte Carlo method. We have shown that the configurational energies of dilute $Fe_{1-x}Cu_x$ computed with the EAM can be reproduced, with an accuracy of 0.04 eV, by a RLM with pair interactions between nearest neighbors (including atom-vacancy interactions). The activation barriers of the vacancy jumps predicted by the EAM potential are reproduced by introducing SP binding energies e_i^{sp} which correspond to the energetic contribution of a jumping i atom when it is at the saddle-point position. Most interestingly, these SP binding energies depend on the nature of the jumping atom and on that of the first neighbors of the SP position: e_i^{sp} can indeed be written as a sum of effective pair interactions between the SP atom and its first neighbors. Note that the dependence of the saddle point-energy on the nature of the surrounding atom is important even in dilute Fe-Cu alloys. Indeed, during the Cu precipitation, the vacancy is often trapped at the precipitate matrix interface. Therefore, the probability of having a Cu atom in a NNSP position is much higher than the Cu concentration.

The previous parameters (pair interactions and SP binding energies) have then been used in MC simulations to study their influence on the diffusion properties and the precipitation kinetics. The dependence of e_{Fe}^{sp} on the SP configuration has no effect on the Fe self-diffusion coefficient and relatively little effect on the Cu impurity diffusion coefficient (which is modified by a factor of 2 or 3 almost independent of the temperature). Nevertheless, by changing the correlation effects between vacancy jumps, it strongly modifies the diffusion coefficient of small copper clusters, especially at low temperature. This affects the competition between two growth processes: individual adsorption of Cu monomers or direct coagulation between copper precipitates.

At high temperature (1000 K) it only modifies the precipitation kinetics by a constant factor on the time scale (however, this factor reaches one order of magnitude). At low temperature (573 K), the sequence of atomic configurations itself is completely modified.

Previous Monte Carlo simulations on rigid lattice have been devoted to the effects of diffusion mechanisms on the kinetics of phase separation in binary *A*-*B* alloys (in the case of simple unmixing[3,4,28,30] or phase ordering[8,9]). However, the conclusions are sometimes rather confusing because these simulations may differ by (i) the elementary diffusion mechanism (e.g., direct exchange between atoms or jump frequencies), (ii) the diffusion barrier used to compute the jump frequencies, and (iii) the MC algorithm (e.g., Metropolis, Glauber, or residence time).

In the first MC studies with diffusion by vacancy jumps it was proposed that the kinetics was almost the same than with direct exchange, except for a constant factor on the time scale.[2] But indeed differences in points (i) and (ii) can completely modify the kinetic pathway of the system. For example, in the case of phase decomposition in highly supersaturated solid solutions (i.e., with a spinodal decomposition behavior), the transient stages before the final coarsening re-

gime differ with vacancy or Kawazaki mechanisms.[4,30]

In many MC simulations[2–4,9,30] the activation barrier is computed as $\Delta E = E_{fin} - E_{ini}$ according to the classical Metropolis scheme (where E_{fin} and E_{ini} are the energies of the system after and before the diffusion event). However, this rule has been developed to study the properties of *equilibrium* states. To study the kinetics of a system which can be, at the beginning of its evolution, very far from the equilibrium, it is more justified to compute the activation barrier according to the rate theory, i.e., with $\Delta E = E_{sp} - E_{ini}$ (where E_{sp} is the energy of the system at the SP position. In the kinetic Ising model (KIM), this is done by writing $E_{sp}^{KIM} = (E_{fin} + E_{ini})/2 + Q$, where the Q parameter is fitted on diffusion data. In the present study, we have rather introduced some e_i^{sp} binding energies at the SP position (as in Refs. 8, 7, 15, and 28). Contrary to the KIM case, there is no *a priori* dependence of E_{sp} and of ΔE on the energy of the *final* state E_{fin}. Moreover, we have seen that this model reproduces the migration barriers computed with the EAM potential. We must emphazised that such differences in the diffusion barriers affect the ratio between the different jump frequencies and hence the kinetic pathway.

One of the key issues of these MC studies is the influence of the details of the *diffusion mechanisms* on the balance between two possible precipitates *growth processes:*[4,8,7,30] (i) the ''emission and adsorption'' of individual B monomers (which is considered, for example, in the classical theory of nucleation or in the Lifschitz-Slyozov-Wagner theory of coarsening[31]); (ii) the ''direct coagulation'' between mobile precipitates (or ''cluster reactions''[32]).

The competition between these two growth processes depends on the details of the simulation in a complicated way. Fratzl and Penrose[4,30] have been one of the first to address this issue: they have compared MC simulations with diffusion by direct A-B exchanges (Kawasaki mechanism) and by vacancy jumps. With the MC parameter they used ($\epsilon_{AA} = \epsilon_{BB}$ and no vacancy-atom interactions), they observed emission-adsorption growth processes when using A-B direct exchanges whereas vacancy jumps lead to the coagulation of small B clusters[30] (with $\epsilon_{AA} = \epsilon_{BB}$ the vacancies are trapped at the precipitate-matrix interfaces and the direct coagulation is actually favored).

However, the elementary diffusion mechanism is not the only control parameter of the balance between the two growth processes. Indeed, for a vacancy jump mechanism, Athènes *et al.*[28] have shown that the correlation effects between successive vacancy jumps and then the relative mobilities of small solute clusters in solid solutions are considerably affected by the ''asymmetry parameter'' $\epsilon_{AA} - \epsilon_{BB}$. It is then possible to modify the balance between emission-adsorption and direct coagulation, keeping the same vacancy jump diffusion mechanism.

These effects have been recently further studied and rationalized by Roussel and Bellon,[6] who have emphasized the role of vacancy trapping. By a suitable choice of the Monte Carlo parameters ($\epsilon_{AA}, \epsilon_{AB}, \epsilon_{BB}$, and $\epsilon_{AV}, \epsilon_{BV}$ if they exist) the vacancy can be trapped in the precipitates, at the precipitate-matrix interfaces, or in the matrix. In the first two cases, as in the simulations of Fratzl and Penrose, the small precipitates are mobile and direct coagulation is observed (the precipitation of Cu in Fe corresponds to this situation). On the contrary in the latter case, the emission and adsorption of monomers is the dominant growth process [as, for example, during the precipitation of Co in Cu (Ref. 6)]. Similar effects had been previously observed by Yaldram and Binder[3] with very high vacancy concentrations ($C_V > 0.04$, i.e., in a case where the vacancies affect not only the kinetics of the A-B system, but its phase diagram too).

Nevertheless, we have shown in this paper that another parameter controls the balance between the growth processes: the SP binding energies. Indeed, changing the saddle-point energies e_i^{sp} does not affect the fraction of time spent by the vacancies in the various phases and interfaces (i.e., the thermodynamic trapping effects). However, during a given time, a vacancy trapped—for example, at an interface—can perform a small number of slow jumps or a big number of fast ones: this effect (which can be simply controlled through e_i^{sp}) modifies the mobility of small clusters and therefore the balance between emission-adsorption and direct coagulation.

The approach proposed in this paper combines the rapidity and simplicity of a RLM to the more realistic energetic description of an EAM potential. One of its advanges is that all the parameters involved in the jump frequencies calculations can be uniquely derived from the EAM potential, while it is usually impossible to find enough reliable experimental data to determine all of them (see the Appendix). As an example, the experimental adjustment of the iron SP binding energy e_{Fe}^{sp} as a function of the local configuration would require knowledge of the Fe and Cu diffusion coefficients in dilute Fe-Cu solid solutions of various compositions. To our knowledge, such measurements are not yet available.

This method can be reasonably extended to other alloys with small size effects (as is the case in the Fe-Cu system), where the interactions are short ranged. However, it may not be straightforwardly used in alloys with strong size effects. Indeed, Bocquet[33] has found that in Au-Ni solid solutions neither the stable configuration energies nor the migration barriers could be reproduced with constant pair interactions (or even with three- or four-body interactions). For this kind of alloy, Monte Carlo simulations with relaxation of the atomic positions, both the stable and the saddle-point ones, have to be performed, but they are much more time consuming than the method proposed in the present study. Therefore such MC simulations are limited to short times (they can be used, for example, to compute tracer diffusion coeffficients[36]). The simulation of longer phenomena (such as precipitation) in the presence of long-range elastic interactions remains possible, even with a vacancy mechanism, but at the cost of the precise description of the activated state.[34]

Of course it would be even better to use *ab initio* calculations rather than empirical potentials. In the case of dilute Fe-Cu alloys the computation of the configurational energies and especially of the various migration barriers, for at least a few different configurations around the saddle-point positions, could become possible in the near future even if the magnetic properties of the iron make the method more difficult.

ACKNOWLEDGMENTS

The authors are grateful to Dr. M. Athènes, Dr. J.-L. Bocquet, Dr. N. V. Doan, Dr. G. Martin, Dr. M. Nastar, and Dr. D. Rodney for stimulating discussions.

APPENDIX: COMPARISON WITH PREVIOUS MONTE CARLO SIMULATIONS

In Ref. 15, Soisson, Barbu, and Martin already proposed a Monte Carlo study of Cu precipitation in α-iron, based on a similar diffusion model, but with stronger approximations. The main differences with the present study are the following.

(i) The parametrization procedure: in Ref. 15, the MC parameters (pair interaction energies, attempt frequencies, SP binding energies) were not derived from an EAM potential, but directly estimated from available experimental data. It was impossible to get ϵ_{CuCu} on a bcc lattice using such a method: this parameter was then kept as a free parameter to fit some precipitation kinetics observed by electrical resistivity measurements.[35]

(ii) For the same reason, it was at that time difficult to get the dependence of the SP binding energies on the local atomic configuration from experimental diffusion data. e_{Fe}^{sp} and e_{Cu}^{sp} were then kept as constant. Furthermore, the same value was chosen for Fe and iron ($e_{Fe}^{sp}=e_{Cu}^{sp}=-8.9$ eV), in order to give a good agreement with experimental self-diffusion and impurity diffusion coefficients.

As a result, by comparison with the present study this former set of parameters (Table II) corresponds to (i) very similar iron self-diffusion and copper impurity diffusion coefficients; (ii) a slightly higher mixing energy ($\omega=-0.18$ eV instead of $\omega=-0.20$ eV for the present simulations): this implies a higher Cu solubility in Fe and a lower precipitation driving force; (iii) almost identical Fe-Fe and Fe-V pair interaction energies (which is quite normal since the EAM potential of Ref. 16 has been fitted on the same cohesive energy and the same vacancy formation energy in iron used to fit the MC parameters of Ref. 15); and (iv) a lower Cu-Cu pair interaction energy and then a larger vacancy formation energy in pure copper [E_V^{for}(Cu) $=2.04$ eV instead of 0.912 eV in our present work].

This last point explains the main difference between the behaviors observed in our present work and in the simulations of Ref. 15: in the latter ones no vacancy trapping was observed in the precipitates (the vacancy concentration was indeed higher in the pure iron matrix than in pure copper precipitates). On the other hand, because the ϵ_{FeCu} parameter is higher than ϵ_{FeFe} and ϵ_{CuCu} (Table II), a vacancy trapping was observed at the Fe/Cu interfaces. But it was less important than in the present simulations and for small precipitate volume fraction it was not sufficient to lead to a significant decrease of the vacancy concentration in the iron matrix [see Fig. 9(b) of Ref. 15]. As a consequence the C_V^{MC}(Fe) $=1/L^3$ was constant in the simulation and the MC time had only to be rescaled by a constant factor.

The precipitation kinetics obtained with the parameters of Ref. 15 (dashed lines) are compared with those of the present work in Figs. 6 and 7: despite the stronger approximations and the differences in thermodynamics and kinetic properties, it is found that the agreement with the kinetics observed in the present simulations (with a configuration-dependent SP binding energy, i.e., DSPE parameters) surprisingly good.

*Present address: Laboratoire d'Étude des Microstructures, CNRS/ONERA, BP 72, 92232 Châtillon Cedex, France.

[1] K. Binder and D. W. Heermann, *Monte Carlo Simulation in Statistical Physics: An Introduction* (Springer, Berlin, 1988).

[2] K. Binder, Rep. Prog. Phys. **60**, 487 (1997); K. Yaldram and K. Binder, Acta Metall. Mater. **39**, 707 (1991).

[3] K. Yaldram and K. Binder, Z. Phys. B: Condens. Matter **81**, 405 (1991).

[4] P. Fratzl and O. Penrose, Phys. Rev. B **50**, 3477 (1994); P. Fratzl, O. Penrose, R. R. Weinkamer, and I. Zizak, Physica A **279**, 100 (2000).

[5] T. T. Rautiainen and A. P. Sutton, Phys. Rev. B **59**, 13 681 (1999).

[6] J.-M. Roussel and P. Bellon, Phys. Rev. B **63**, 184114 (2001).

[7] F. Soisson and G. Martin, Phys. Rev. B **62**, 203 (2000).

[8] M. Athènes, P. Bellon, G. Martin, and F. Haider, Acta Mater. **44**, 4739 (1996); M. Athènes, P. Bellon, and G. Martin, Philos. Mag. A **76**, 527 (1997); M. Athènes and P. Bellon, *ibid.* **79**, 2243 (1999).

[9] E. Vives and A. Planes, Phys. Rev. Lett. **68**, 812 (1992); Phys. Rev. B **47**, 2557 (1993); C. Frontera, E. Vives, T. Castán, and A. Planes, *ibid.* **48**, 9321 (1993).

[10] M. Athènes, F. Soisson, P. Bellon, and G. Martin, in *Proceedings of the International Conference on Solid-Solid Phase Transformations 99*, edited by M. Koiwa, K. Otsuka, and T. Miyazaki (The Japan Institute of Metals, Sendai, 1999), p. 433.

[11] P. J. Othen, M. L. Jenkins, and G. D. Smith, Philos. Mag. A **70**, 1 (1994).

[12] T. Kraft, P. M. Marcus, M. Methfessel, and M. Scheffler, Phys. Rev. B **48**, 5886 (1993).

[13] S. Jeong, Phys. Rev. B **53**, 13 973 (1996).

[14] L. G. Wang, and M. Sob, Phys. Rev. B **60**, 844 (1999).

[15] F. Soisson, A. Barbu, and G. Martin, Acta Mater. **44**, 3789 (1996).

[16] M. Ludwig, D. Farkas, D. Pedraza, and S. Schmauder, Modell. Simul. Mater. Sci. Eng. **6**, 19 (1998).

[17] G. J. Ackland, D. J. Bacon, A. F. Calder, and T. Harry, Philos. Mag. A **75**, 713 (1997).

[18] Yu. N. Osetsky, S. I. Golubov, and A. Serra, Defect Diffus. Forum **143-147**, 505 (1997).

[19] Y. Le Bouar, Acta Mater. **49**, 2661 (2001).

[20] J. J. Blackstock and G. J. Ackland, Philos. Mag. A **81**, 2127 (2001).

[21] A. Seeger, Phys. Status Solidi A **167**, 289 (1998).

[22] G. Salje and M. Feller-Kniepmeier, J. Appl. Phys. **48**, 1833 (1977).

[23] J.-L. Bocquet, G. Brebec, and Y. Limoge, in *Physical Metallurgy*, edited by R. W. Cahn and P. Haasen (North-Holland, Amsterdam, 1996), Chap. 7.

[24] L. Zhao, R. Najafabadi, and D. J. Srolovitz, Acta Mater. **44**, 2737 (1996).

[25] G. Henkelman, G. Johannesson, and H. Jonsson, in *Progress on Theoretical Chemistry and Physics*, edited by S. D. Schwartz (Kluwer Academic, Dordrecht, 2000).
[26] Y. Le Bouar and S. Walle, Defect Diffus. Forum **194-199**, 139 (2001).
[27] A. D. Le Claire, in *Physical Chemistry: An Advanced Treatise*, edited by H. Eyring (Academic Press, New York, 1970), Vol. 10, Chap. 5.
[28] M. Athènes, P. Bellon, and G. Martin, Acta Mater. **48**, 2675 (2000).
[29] *Numerical Data and Functional Relationships in Science and Technology*, edited by H. Mehrer, Landolt-Börnstein, New Series, Vol. 26 (Springer-Verlag, Berlin, 1990).
[30] P. Fratzl and O. Penrose, Phys. Rev. B **55**, R6101 (1997).
[31] I. M. Lifschitz, V. V. Slyozov, J. Phys. Chem. Solids **19**, 35 (1961); C. Wagner, Z. Elektrochem. **65**, 243 (1961).
[32] K. Binder and D. Stauffer, Phys. Rev. Lett. **33**, 1006 (1974).
[33] J.-L. Bocquet (private communication).
[34] A. Finel, in *Phase Transformations and Evolution in Materials*, edited by P. E. A. Turchi and A. Gonis (TMS, Warrendale, 2000) p. 371.
[35] T.N. Lâe, A. Barbu, and F. Maury, Scr. Metall. Mater. **26**, 771 (1992).
[36] J.L. Bocquet and C. Schmidt, Defect Diffus. Forum **194-199**, 145 (2001).
[37] E_{Cu}^{sol} is the energy of a simulation box containing $(N-1)$ Fe atoms and one substitutional Cu impurity minus the cohesive energy of $(N-1)$ Fe atoms in a perfect bcc crystal, minus the cohesive energy of 1 Cu atom in a fcc crystal.
[38] The critical size i^* has been computed from the balance between the precipitation driving force and the interfacial energy between the matrix and precipitates, in the framework of the classical theory of nucleation (CTN). The link between these quantities and the MC parameters is explained in Ref. 7. However, the initial solid solution is highly supersaturated and the critical size is very small ($i^*=1$ for $T=573$ K and $x=3\%, i^*=2$ for $T=1000$ K and $x=1\%$) and a small error in the estimation from the CTN will not strongly affect the values of N_p ($i>i^*$) and $\langle i \rangle$.